




Article

First-Principles Study of Thermo-Physical Properties of Pu-Containing $Gd_2Zr_2O_7$

Pengcheng Li ¹, Fengai Zhao ², Haiyan Xiao ^{1,*}, Haibin Zhang ^{3,*}, Hengfeng Gong ⁴, Sa Zhang ¹, Zijiang Liu ⁵  and Xiaotao Zu ^{1,2}

¹ School of Physics, University of Electronic Science and Technology of China, Chengdu 610054, China; pengchengli257335@gmail.com (P.L.); 15136231837@163.com (S.Z.); xtzu@uestc.edu.cn (X.Z.)

² Institute of Fundamental and Frontier Sciences, University of Electronic Science and Technology of China, Chengdu 610054, China; fengaizh0506@163.com

³ Institute of Nuclear Physics and Chemistry, Chinese Academy of Engineering Physics, Mianyang 621900, China

⁴ Department of ATF R&D, China Nuclear Power Technology Research Institute Co., Ltd., Shenzhen 518000, China; gonghengfeng@cgnpc.com.cn

⁵ Department of Physics, Lanzhou City University, Lanzhou 730070, China; lzjcaep@126.com

* Correspondence: hyxiao@uestc.edu.cn (H.X.); hbzhang@imr.ac.cn (H.Z.); Tel.: +86-28-83202130 (H.X.); +86-816-2480282 (H.Z.)

Received: 2 January 2019; Accepted: 31 January 2019; Published: 3 February 2019



Abstract: A density functional theory plus Hubbard U method is used to investigate how the incorporation of Pu waste into $Gd_2Zr_2O_7$ pyrochlore influences its thermo-physical properties. It is found that immobilization of Pu at Gd-site of $Gd_2Zr_2O_7$ has minor effects on the mechanical and thermal properties, whereas substitution of Pu for Zr-site results in remarkable influences on the structural parameters, elastic moduli, elastic isotropy, Debye temperature and electronic structure. The discrepancy in thermo-physical properties between $Gd_{2-y}Pu_yZr_2O_7$ and $Gd_2Zr_{2-y}Pu_yO_7$ may be a result of their different structural and electronic structures. This study provides a direct insight into the thermo-physical properties of Pu-containing $Gd_2Zr_2O_7$, which will be important for further investigation of nuclear waste immobilization by pyrochlores.

Keywords: DFT+U; $Gd_2Zr_2O_7$; nuclear waste; mechanical properties

1. Introduction

As the nuclear industry develops fast, ways to treat spent fuel and nuclear waste safely, such as plutonium and minor actinides (Np, Am, Cm), has become an important environmental conservation issue [1–3]. It is acceptable to store spent fuel and separated waste in stainless steel vessels in the short term, but in the long term it is hoped that this material will be transformed into more secure and manageable solids [1,4,5]. One method proposed for the treatment of plutonium is immobilization in zirconate pyrochlores, particularly $Gd_2Zr_2O_7$, which has high thermal stability, high chemical durability, and high radiation tolerance [6–9]. Besides, Gd is an effective neutron absorber [6].

Experimentally, Pu is often substituted by nonradioactive cerium (Ce), since they share the same crystallographic structure, and thermo-physical and chemical properties [10,11]. Zhao et al. synthesized $(Gd_{1-x}Ce_x)_2Zr_2O_{7+x}$ ($0 \leq x \leq 0.6$) solid solutions, indicating that Ce^{3+} ions can be incorporated into the Gd^{3+} sites. They proposed that the content of Pu^{3+} immobilized at Gd-site was less than 40 mol% [12]. On the other hand, $Gd_2(Zr_{1-x}Ce_x)_2O_7$ ($0 \leq x \leq 1.0$) solid solutions have been synthesized by Reid et al. [13] and Patwe et al. [14]. They found that Ce can be immobilized at Zr sites entirely as Ce^{4+} , which leads to structural transformation from pyrochlore to fluorite phase, and its composition ranges from $Gd_2Ce_{0.2}Zr_{1.8}O_7$ to $Gd_2Ce_{1.7}Zr_{0.3}O_7$. Similar solution behavior

and structural properties for Pu incorporation in $\text{Gd}_2\text{Zr}_2\text{O}_7$ have been obtained by first-principles calculations [15–17]. However, different electronic structures can be obtained for Ce and Pu immobilization at the Gd-site of $\text{Gd}_2\text{Zr}_2\text{O}_7$, i.e., the band gap increases and reduces when Ce and Pu substitutes for Gd site, respectively [15,18]. These differences mainly result from the different <Ce-O> and <Pu-O> interactions at band edges. The different electronic structure may result in varying mechanical properties. For Young's modulus, which is described by $E \propto \frac{M_a}{r_0^4}$, with M_a the Madelung constant and r_0 the interionic spacing [19], it is very sensitive to r_0 . For ionic crystals, the r_0 is affected by bond interactions. According to these analyses, large discrepancies in electronic structures between Ce and Pu incorporation in $\text{Gd}_2\text{Zr}_2\text{O}_7$ may lead to different Young's modulus. This indicates that for the mechanical properties of pyrochlores, Ce may not be a good substitute for Pu, despite the two having several similar thermo-physical properties. Thus far, there are no reports on the mechanical properties of Pu immobilization in $\text{Gd}_2\text{Zr}_2\text{O}_7$. It is necessary to explore how Pu doping influences the mechanical properties of $\text{Gd}_2\text{Zr}_2\text{O}_7$, because the knowledge of thermo-mechanical characteristics, for example, elastic moduli and Debye temperature is important for safe fuel disposal [20]. It provides new perspectives into the behavior of actinide incorporation in pyrochlores for their applications in harsh environments.

In this work, the structural, mechanical and electronic properties of Pu incorporation in $\text{Gd}_2\text{Zr}_2\text{O}_7$ are investigated by the density functional theory plus the Hubbard U method (DFT+U). The remaining part of the paper is structured as follows: Section 2 lists computational details; Section 3 contains our results and discussions, involving the structural stability, elastic constants with elastic moduli of $\text{Gd}_{2-y}\text{Pu}_y\text{Zr}_2\text{O}_7$ and $\text{Gd}_2\text{Zr}_{2-y}\text{Pu}_y\text{O}_7$, as well as the ductility, elastic anisotropy, Debye temperature and electronic structures of Pu-doped $\text{Gd}_2\text{Zr}_2\text{O}_7$. In Section 4, we summarize our conclusions.

2. Computational Details

The density functional theory method within the Vienna *Ab-initio* Simulation Package (VASP) [21,22] are employed in all the computations. The Hubbard U correction [23] is considered to take into account the strong correlation interaction between 5f electrons of Pu and the effective U values are taken to be 4 eV. The projector augmented wave (PAW) method [24] is used to describe the interaction between electrons and ions. As for the exchange-correlation functional, a number of generalized gradient approximation (GGA) functionals have been reported in the literature [25–27] and the functional parametrized by Perdew, Burke and Ernzerhof [28] is employed in this work. In the calculations, a $2 \times 2 \times 2$ k-point sampling in reciprocal space is employed, with a cutoff energy of 600 eV for the plane wave basis sets. Figure 1 illustrates the schematic view of geometrical structure for the considered compounds, i.e., $\text{Gd}_{2-y}\text{Pu}_y\text{Zr}_2\text{O}_7$ and $\text{Gd}_2\text{Zr}_{2-y}\text{Pu}_y\text{O}_7$ ($y = 0, 0.5, 1.0, 1.5, 2.0$). The special quasi-random structure method is used to build the structural models for Pu immobilization at Gd-site and Zr-site [29–32].

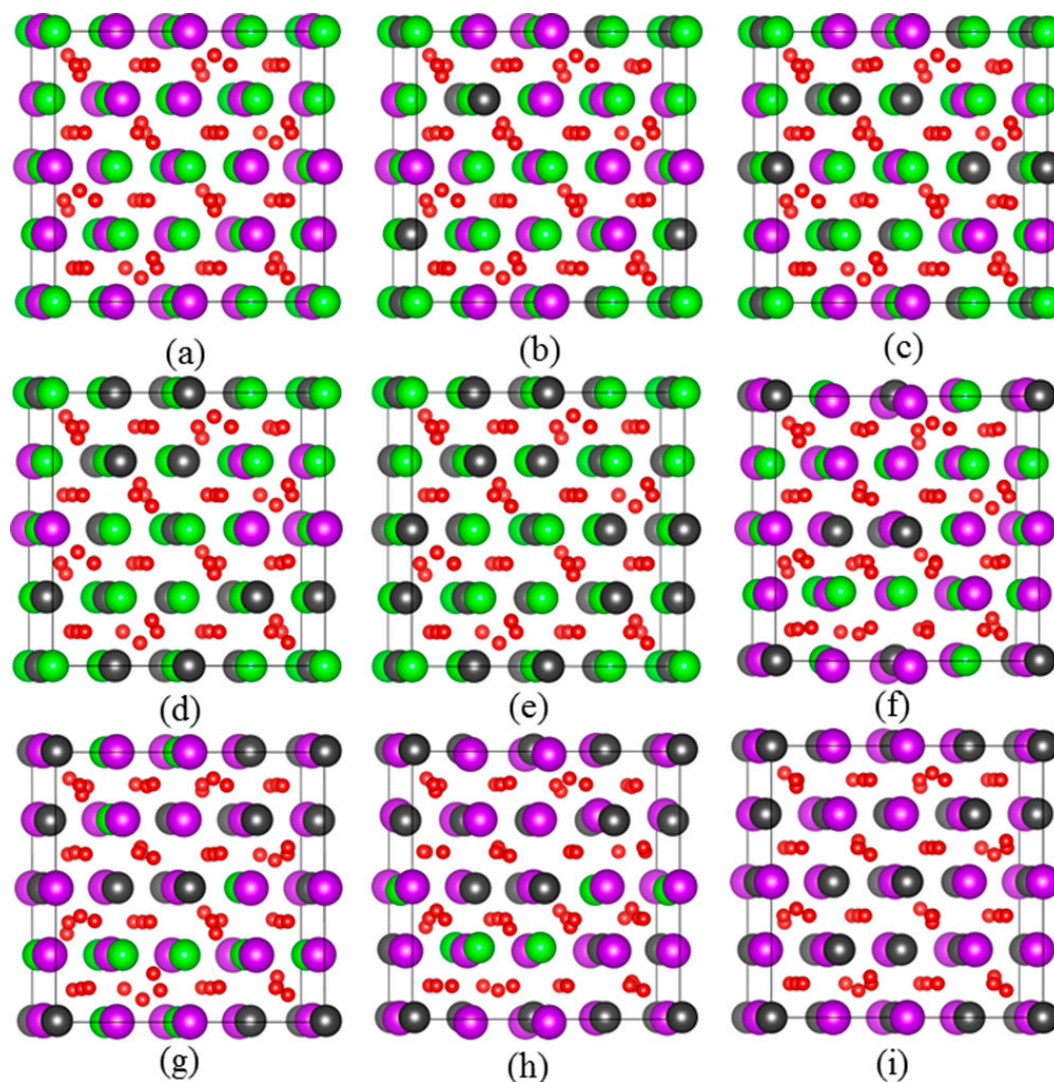


Figure 1. Schematic views of optimized geometrical structures for: (a) $Gd_2Zr_2O_7$; (b) $Gd_{1.5}Pu_{0.5}Zr_2O_7$; (c) $Gd_{1.0}Pu_{1.0}Zr_2O_7$; (d) $Gd_{0.5}Pu_{1.5}Zr_2O_7$; (e) $Pu_2Zr_2O_7$; (f) $Gd_2Zr_{1.5}Pu_{0.5}O_7$; (g) $Gd_2Zr_{1.0}Pu_{1.0}O_7$; (h) $Gd_2Zr_{0.5}Pu_{1.5}O_7$; (i) $Gd_2Pu_2O_7$. The purple, dark grey, green and red spheres represent Gd, Pu, Zr and O atoms, respectively. (For interpretation of the references to color in this figure legend, the reader is referred to the web version of this article.)

3. Results and Discussion

3.1. Structural Stability of Pu Incorporation into $Gd_2Zr_2O_7$

As Pu substitutes for Gd^{3+} and Zr^{4+} in $Gd_2Zr_2O_7$, the corresponding valence states for Pu are Pu^{3+} and Pu^{4+} , respectively. Because in both PuO_2 and Pu_2O_3 the Pu 5f electrons are strongly correlated, Hubbard U correction is thus necessary. In the revised manuscript, we present the density of state distribution for both PuO_2 and Pu_2O_3 at $U_{eff} = 0$ eV and $U_{eff} = 4$ eV in Figure 2. It is shown that without Hubbard U correction, i.e., at $U_{eff} = 0$ eV, the Pu 5f electrons are itinerant and delocalized over the Fermi level, resulting in metallic states. At $U_{eff} = 4$ eV, the Pu 5f electrons are localized and the system becomes insulating, which is consistent with the experimental finding [32]. The calculated lattice constant of 5.46 Å for PuO_2 and 11.18 Å for Pu_2O_3 obtained at $U_{eff} = 4$ eV are comparable to the experimental values of 5.39 Å [33] and 10.98 Å [34], respectively. The calculated band gap for Pu_2O_3 at $U_{eff} = 4$ eV is 1.757 eV, which corresponds to the experimental value of 2 eV [35]. Thus, we use

$U_{\text{eff}} = 4$ eV in our subsequent calculations for Pu immobilization in $\text{Gd}_2\text{Zr}_2\text{O}_7$. On the other hand, the 4 eV for U_{eff} is also consistent with the value of 4–5 eV that are reported in the literature [36,37].

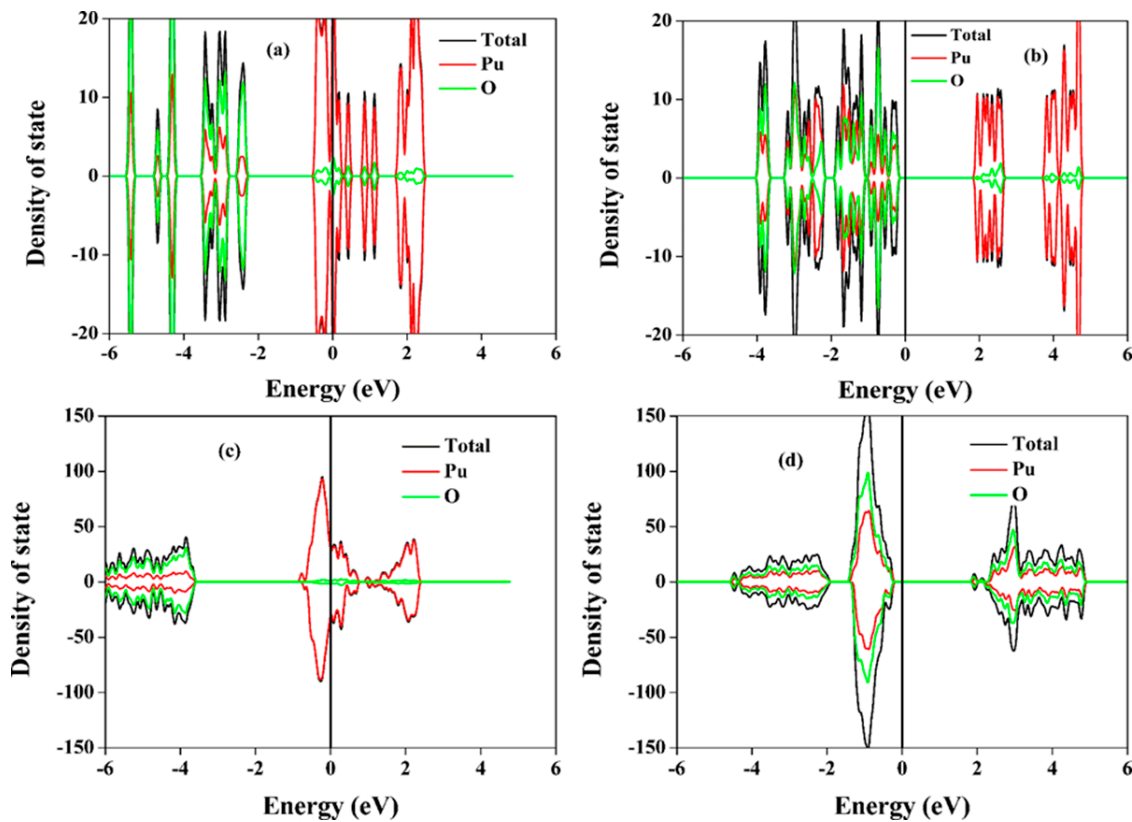


Figure 2. Density of state distribution for PuO_2 at (a) $U_{\text{eff}} = 0$ eV and (b) 4 eV and for Pu_2O_3 at (c) $U_{\text{eff}} = 0$ eV and (d) 4 eV obtained by GGA+U.

A structural optimization is first performed for both $\text{Gd}_{2-y}\text{Pu}_y\text{Zr}_2\text{O}_7$ and $\text{Gd}_2\text{Zr}_{2-y}\text{Pu}_y\text{O}_7$. The calculated lattice constants, oxygen positional parameter $x_{\text{O}48f}$ and bond distances for $\text{Gd}_{2-y}\text{Pu}_y\text{Zr}_2\text{O}_7$ and $\text{Gd}_2\text{Zr}_{2-y}\text{Pu}_y\text{O}_7$ are listed in Tables 1 and 2, respectively. The changes of lattice constant and $x_{\text{O}48f}$ for $\text{Gd}_{2-y}\text{Pu}_y\text{Zr}_2\text{O}_7$ and $\text{Gd}_2\text{Zr}_{2-y}\text{Pu}_y\text{O}_7$ with Pu concentrations are shown in Figure 3. The calculated lattice constant of 10.666 Å for $\text{Gd}_2\text{Zr}_2\text{O}_7$ is slightly larger than the experimental value of 10.54 Å [38], while consistent with other calculations of 10.66 Å [18]. The calculated a_0 of 10.802 Å for $\text{Pu}_2\text{Zr}_2\text{O}_7$ is comparable with the experimental value of 10.70 Å [39]. As the Pu content increases, the lattice constant gradually increases for both $\text{Gd}_{2-y}\text{Pu}_y\text{Zr}_2\text{O}_7$ and $\text{Gd}_2\text{Zr}_{2-y}\text{Pu}_y\text{O}_7$, and it changes more significantly for $\text{Gd}_2\text{Zr}_{2-y}\text{Pu}_y\text{O}_7$ than that for $\text{Gd}_{2-y}\text{Pu}_y\text{Zr}_2\text{O}_7$. This is caused by the fact that the effective ionic radius of 1.053 Å [40] for Gd^{3+} is in good agreement with the value of ~ 1.1 Å [40] for Pu^{3+} , but the effective ionic radius of 0.72 Å [40] for Zr^{4+} is much smaller than the value of 0.96 Å [40] for Pu^{4+} . With regard to oxygen positional parameter $x_{\text{O}48f}$, the calculated value of 0.339 for $\text{Gd}_2\text{Zr}_2\text{O}_7$ is smaller than the experimental value of 0.345 [41], and is comparable to the calculated value of 0.339 reported by Wang et al. [18]. For $\text{Gd}_{2-y}\text{Pu}_y\text{Zr}_2\text{O}_7$, the $x_{\text{O}48f}$ changes slightly as the Pu content increases, which indicates that the $\text{Gd}_{2-y}\text{Pu}_y\text{Zr}_2\text{O}_7$ remains the pyrochlore structure. Wang et al. [18] has observed similar phenomenon for $\text{Gd}_{2-y}\text{Ce}_y\text{Zr}_2\text{O}_7$. For $\text{Gd}_2\text{Zr}_{2-y}\text{Pu}_y\text{O}_7$, we find that the $x_{\text{O}48f}$ increases a lot, varying from 0.339 to 0.350, suggesting that the $\text{Gd}_2\text{Zr}_{2-y}\text{Pu}_y\text{O}_7$ tends to be a defect fluorite structure as the Pu content increases [15]. Comparing the lattice constant and oxygen positional parameter for $\text{Gd}_{2-y}\text{Pu}_y\text{Zr}_2\text{O}_7$ and $\text{Gd}_2\text{Zr}_{2-y}\text{Pu}_y\text{O}_7$, we find that the formation of $\text{Gd}_2\text{Zr}_2\text{O}_7$ - $\text{Pu}_2\text{Zr}_2\text{O}_7$ solid solution is more preferable than that of $\text{Gd}_2\text{Zr}_2\text{O}_7$ and $\text{Gd}_2\text{Pu}_2\text{O}_7$. As for bond distances, the calculated $\langle \text{Gd}-\text{O}_{48f} \rangle$ distance of 2.553 Å in $\text{Gd}_2\text{Zr}_2\text{O}_7$ is a little larger than the experimental value of 2.483 Å [38],

and is comparable to other calculated value of 2.548 Å [18]. Meanwhile, the calculated value of 2.109 Å for $\langle \text{Zr-O}_{48f} \rangle$ distance is consistent with the experimental value [38] and other calculated value [18] of 2.110 Å. For $\text{Gd}_{2-y}\text{Pu}_y\text{Zr}_2\text{O}_7$, the $\langle \text{Gd-O}_{48f} \rangle$ and $\langle \text{Pu-O}_{48f} \rangle$ distances increase slightly and the $\langle \text{Gd-O}_{8b} \rangle$ and $\langle \text{Pu-O}_{8b} \rangle$ distances decrease slightly as the Pu content increases. Comparing the $\langle \text{Gd-O} \rangle$ and $\langle \text{Pu-O} \rangle$ bonds, we find that the $\langle \text{Pu-O}_{48f} \rangle$ and $\langle \text{Pu-O}_{8b} \rangle$ distances are slightly larger than $\langle \text{Gd-O}_{48f} \rangle$ and $\langle \text{Gd-O}_{8b} \rangle$ distances, respectively, i.e., Pu substitution for Gd-site leads to small increase in the bonding distance. For $\text{Gd}_2\text{Zr}_{2-y}\text{Pu}_y\text{O}_7$, the situation is different. The $\langle \text{Pu-O}_{48f} \rangle$ bond is about 0.12–0.19 Å larger than the $\langle \text{Zr-O}_{48f} \rangle$ bond. Simultaneously, the $\langle \text{Gd-O}_{8b} \rangle$ bond increases a little as the Pu content increases. Consequently, there is a remarkable increase in the lattice constant of $\text{Gd}_{2-y}\text{Pu}_y\text{Zr}_2\text{O}_7$.

Table 1. Lattice constant a_0 (Å), O_{48f} positional parameter x and bond distances (Å) for $\text{Gd}_{2-y}\text{Pu}_y\text{Zr}_2\text{O}_7$. Eg represents the band gap.

	a_0	$x_{O_{48f}}$	E_g (eV)	$d\langle \text{Gd-O}_{48f} \rangle$	$d\langle \text{Gd-O}_{8b} \rangle$	$d\langle \text{Pu-O}_{48f} \rangle$	$d\langle \text{Pu-O}_{8b} \rangle$	$d\langle \text{Zr-O}_{48f} \rangle$
y = 0	10.666	0.339	2.86	2.553	2.309	-	-	2.109
Exp.	10.540 [38]	0.345 [41]		2.483 [38]				
Cal.	10.66 [18]	0.339 [18]		2.548 [18]	2.307 [18]			2.110 [18]
y = 0.5	10.703	0.337	2.33	2.561	2.302	2.582	2.369	2.111
y = 1.0	10.736	0.337	2.27	2.578	2.284	2.591	2.366	2.114
y = 1.5	10.768	0.336	2.33	2.574	2.286	2.605	2.349	2.116
y = 2.0	10.802	0.335	2.37	-	-	2.615	2.339	2.117
Exp.	10.70 [39]							

Table 2. Lattice constant a_0 (Å), O_{48f} positional parameter x and bond distances (Å) for $\text{Gd}_2\text{Zr}_{2-y}\text{Pu}_y\text{O}_7$. Eg represents the band gap.

	a_0	$x_{O_{48f}}$	E_g (eV)	$d\langle \text{Gd-O}_{48f} \rangle$	$d\langle \text{Gd-O}_{8b} \rangle$	$d\langle \text{Pu-O}_{48f} \rangle$	$d\langle \text{Zr-O}_{48f} \rangle$
y = 0	10.666	0.339	2.86	2.553	2.309	-	2.109
Exp.	10.540 [38]	0.345 [41]		2.483 [38]			
Cal.	10.66 [18]	0.339 [18]		2.548 [18]	2.307 [18]		2.110 [18]
y = 0.5	10.750	0.342	2.33	2.513	2.338	2.296	2.110
y = 1.0	10.836	0.344	1.99	2.555	2.347	2.228	2.114
y = 1.5	10.909	0.350	1.68	2.508	2.364	2.273	2.121
y = 2.0	11.003	0.350	1.75	2.552	2.382	2.234	-

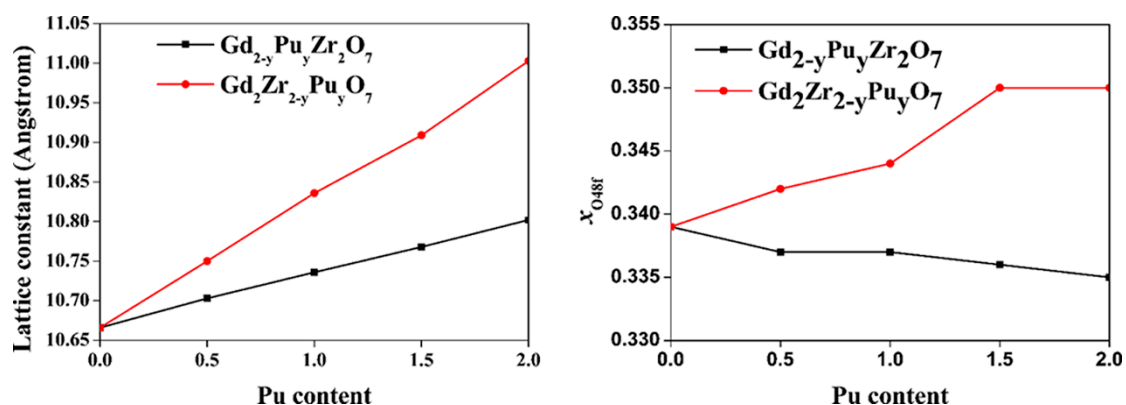


Figure 3. Variation of (a) lattice constant and (b) $x_{O_{48f}}$ for $\text{Gd}_{2-y}\text{Pu}_y\text{Zr}_2\text{O}_7$ and $\text{Gd}_2\text{Zr}_{2-y}\text{Pu}_y\text{O}_7$ with Pu content. The calculated and fitted results are represented by symbols and dashed lines, respectively.

3.2. Elastic Constants and Elastic Moduli of $\text{Gd}_{2-y}\text{Pu}_y\text{Zr}_2\text{O}_7$ and $\text{Gd}_2\text{Zr}_{2-y}\text{Pu}_y\text{O}_7$

Elastic constants are response functions to the external forces and are very important in the materials' properties [42]. Table 3 lists the calculated elastic constants along with available experimental and theoretical values. For $\text{Gd}_2\text{Zr}_2\text{O}_7$, the calculated C_{11} , C_{12} and C_{44} are 285.1, 102.5 and 82.1 GPa, respectively, showing good agreement with other calculations [43]. For $\text{Pu}_2\text{Zr}_2\text{O}_7$, the calculated

$C_{11} = 270.6$ GPa, $C_{12} = 107.3$ GPa and $C_{44} = 81.2$ GPa differ from reference [2], in which different calculational parameters are employed. It is noted that the elastic stability criteria are satisfied for all the investigated systems, i.e., $C_{11} > |C_{12}|$, $C_{44} > 0$, and $(C_{11} + 2C_{12}) > 0$ [44], implying that they are all mechanically stable.

Table 3. Elastic constants (C_{11} , C_{12} , C_{44} , in GPa), bulk modulus B (GPa), shear modulus G (GPa), Young's modulus E (GPa) of $Gd_{2-y}Pu_yZr_2O_7$ and $Gd_2Zr_{2-y}Pu_yO_7$ ($0 \leq y \leq 2$).

		C_{11}	C_{12}	C_{44}	B	G	E
$Gd_2Zr_2O_7$		285.1	102.5	82.1	163.4	85.7	218.8
	Cal [43]	289	103	85	165	88	224
	Exp [45,46]				153	80	205
	Exp [20]				174	92	236
$Gd_{1.5}Pu_{0.5}Zr_2O_7$		282.6	105.1	82.7	164.3	85.1	217.6
$Gd_{1.0}Pu_{1.0}Zr_2O_7$		278.1	106.9	83.1	164.0	84.1	215.4
$Gd_{0.5}Pu_{1.5}Zr_2O_7$		274.9	107.2	82.5	163.1	83.0	213.0
$Pu_2Zr_2O_7$		270.6	107.3	81.2	161.7	81.4	209.1
	Cal [2]	306	131.8	90.2			
$Gd_2Zr_{1.5}Pu_{0.5}O_7$		251.9	86.3	67.7	141.5	73.4	187.7
$Gd_2Zr_{1.0}Pu_{1.0}O_7$		235.2	83.8	49.8	134.3	58.9	154.2
$Gd_2Zr_{0.5}Pu_{1.5}O_7$		242.8	92.0	56.5	142.3	63.4	165.7
$Gd_2Pu_2O_7$		234.8	87.9	57.8	136.9	63.6	165.3

Figure 4 presents the changes of elastic constants with Pu content for both $Gd_{2-y}Pu_yZr_2O_7$ and $Gd_2Zr_{2-y}Pu_yO_7$. For $Gd_{2-y}Pu_yZr_2O_7$, as the Pu content increases, the elastic constants are affected minorly. As the Pu concentration increases, the C_{11} and C_{12} decreases and increases slightly, respectively, and the change in C_{44} , is nearly negligible. As for $Gd_2Zr_{2-y}Pu_yO_7$, the variation of elastic constants with Pu content is more considerable. As the y value changes, the C_{11} and C_{12} first decreases, then increases, and finally decreases again. As for C_{44} , it first decreases to $y = 1.5$, and then increases. Generally speaking, as the Pu content increases, there are more significant changes on Zr-site than Gd-site, meaning that Pu immobilization at Zr-site leads to remarkable variations in the mechanical properties of $Gd_2Zr_2O_7$. Zhao et al. [47] also reported that Nd substitution of Zr-site of $Gd_2Zr_2O_7$ greatly affects the mechanical properties.

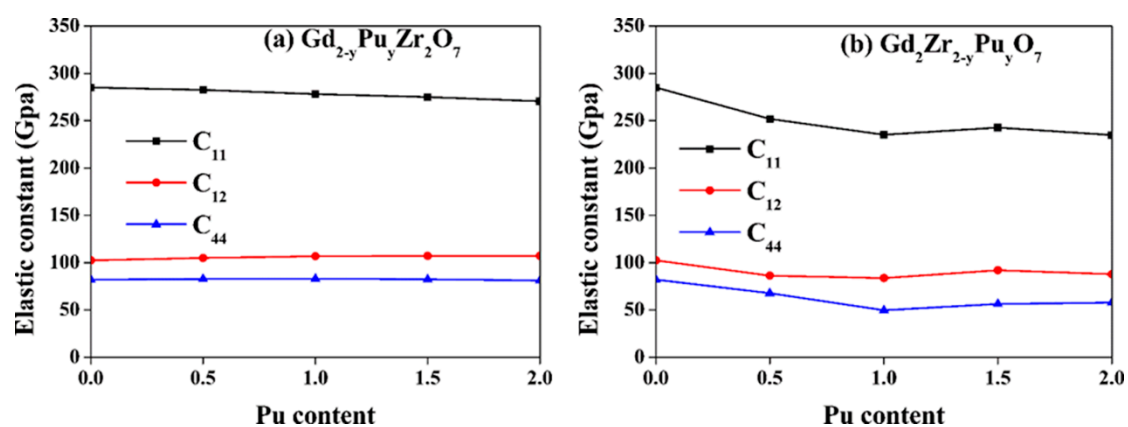


Figure 4. Variation of elastic constants (C_{11} , C_{12} and C_{44}) for (a) $Gd_{2-y}Pu_yZr_2O_7$ and (b) $Gd_2Zr_{2-y}Pu_yO_7$ ($0 \leq y \leq 2$) with Pu content.

From the calculated elastic constants, the elastic moduli, including the bulk modulus (B), shear modulus (G) and Young's modulus (E), can be deduced [48–51], i.e.,

$$B = B^V = B^R = \frac{C_{11} + 2C_{12}}{3},$$

$$G^V = \frac{C_{11} - C_{12} + 3C_{44}}{5},$$

$$G^R = \frac{5(C_{11} - C_{12})C_{44}}{4C_{44} + 3(C_{11} - C_{12})},$$

$$G = G^{VRH} = \frac{G^V + G^R}{2},$$

$$E = \frac{9BG}{3B + G}.$$

Here, the Voigt and Reuss evaluations for B and G are represented by V and R , respectively. Table 3 lists the calculated B , G , E , and others' theoretical and experimental values for both $Gd_{2-y}Pu_yZr_2O_7$ and $Gd_2Zr_{2-y}Pu_yO_7$. For $Gd_2Zr_2O_7$, the calculated $B = 163.4$ GPa, $G = 85.7$ GPa, $E = 218.8$ GPa are comparable with experimental [20,45,46] and other calculated [43] results. Figure 5 shows the variation of elastic moduli for both $Gd_{2-y}Pu_yZr_2O_7$ and $Gd_2Zr_{2-y}Pu_yO_7$. For $Gd_{2-y}Pu_yZr_2O_7$, the elastic moduli change very slightly as the Pu content increases. When Pu is immobilized at Zr-site, there are remarkable changes. The bulk modulus first decreases, reaching a minimum of 134.3 GPa at $y = 1.0$, then rises up to 142.3 GPa at $y = 1.5$ and finally decreases to 136.9 GPa at $y = 2.0$. The shear modulus decreases to 58.9 GPa at $y = 1.0$ and increases slightly to 63.6 GPa at $y = 2.0$. The Young's modulus decreases sharply from 218.8 GPa to 154.2 GPa as the y varies from 0 to 1.0, but increases again to 165.7 GPa at $y = 1.5$, finally changing slightly. The $\langle Zr-O \rangle$ bonds determine the total stiffness of $A_2Zr_2O_7$ pyrochlore, because the corner-sharing ZrO_6 octahedra constitutes its backbone, and the A^{3+} fills the interstices [19,52]. Therefore, the substitution of Zr^{4+} by Pu^{4+} causes the change of $\langle Zr-O \rangle$ bonds to $\langle Pu-O \rangle$ bonds and influences the Young's modulus, especially for these ionic bonds [19,52]. The Young's modulus E is described by $E \propto \frac{M_a}{r_0^4}$ for ionic bonds, in which M_a represents the Madelung constant and r_0 represents the interionic distance [19]. The $\langle Zr-O \rangle$ bonds in $Gd_2Zr_2O_7$ are affected little by Pu substitution for Gd-site, leading to slight effects on the Young's modulus. For $Gd_2Zr_{2-y}Pu_yO_7$, the $\langle Zr-O_{48f} \rangle$ bond length of 2.11 Å is smaller than the value of 2.26 Å for $\langle Pu-O_{48f} \rangle$, resulting in remarkable effects on the Young's modulus. The bulk modulus, shear modulus and Young's modulus for Nd doping of $Gd_2Zr_2O_7$ have been calculated by Zhao et al. [47], who also reported that Nd immobilization at Zr-site has more remarkable influences on the elastic moduli than that at Gd-site.

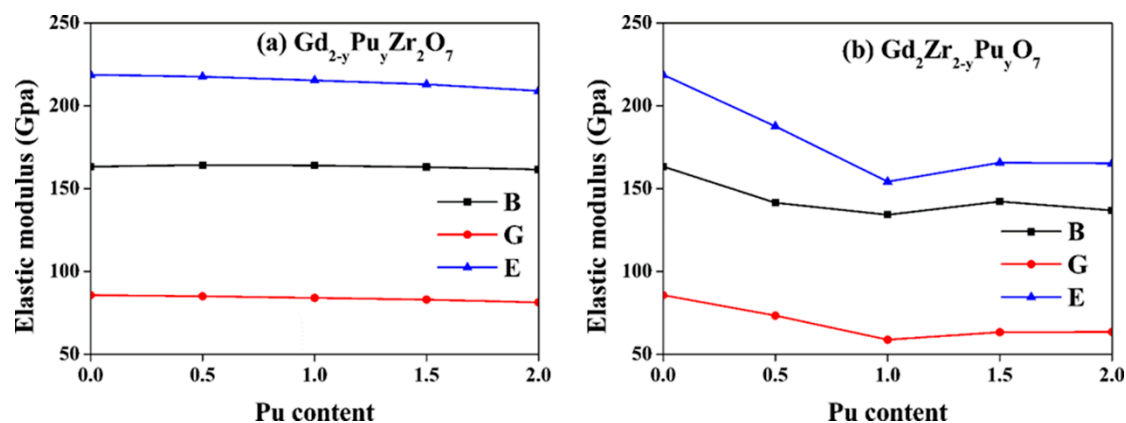


Figure 5. Variation of elastic moduli for (a) $Gd_{2-y}Pu_yZr_2O_7$ and (b) $Gd_2Zr_{2-y}Pu_yO_7$ ($0 \leq y \leq 2$) as a function of Pu content. B : bulk modulus; G : shear modulus; E : Young's modulus.

For each ion in $Gd_{2-y}Pu_yZr_2O_7$ and $Gd_2Zr_{2-y}Pu_yO_7$, we analyze the Bader charge to explore the origin of the discrepancy in the elastic moduli between $Gd_{2-y}Pu_yZr_2O_7$ and $Gd_2Zr_{2-y}Pu_yO_7$. The Bader charge values are listed in Table 4. As Pu is immobilized at Gd-site and Zr-site, the average Bader charge for Pu are 2.10 |e| and 2.33 |e|, respectively, corresponding to the nominal +3 |e| and +4 |e| in oversimplified classical model [2]. For $Gd_{2-y}Pu_yZr_2O_7$, the Bader charge for Gd and Pu ions are similar to each other, i.e., 2.15 and 2.10 |e|, respectively. Wang et al. [18] calculated the Bader charge of $Gd_{2-y}Ce_yZr_2O_7$ and reported very similar results. Additionally, the bonding distance for $\langle Gd-O_{48f} \rangle$ and $\langle Gd-O_{8b} \rangle$ are determined to be 2.57 Å and 2.30 Å, which are comparable to the values of 2.60 Å for $\langle Pu-O_{48f} \rangle$ and 2.36 Å for $\langle Pu-O_{8b} \rangle$, respectively. Obviously, the $\langle Gd-O \rangle$ and $\langle Pu-O \rangle$ bonding interaction are very similar to each other, which explains why the mechanical properties of $Gd_2Zr_2O_7$ are affected slightly by Pu immobilization at Gd-site. For $Gd_2Zr_{2-y}Pu_yO_7$, the situation is much different. The average Bader charge are 2.33 |e| for Pu ions and 2.26 |e| for Zr ions. Considering that the $\langle Pu-O_{48f} \rangle$ distance of 2.26 Å is larger than the $\langle Zr-O_{48f} \rangle$ distance of 2.11 Å and the ionic radius of 0.96 Å for Pu ions is larger than that of 0.72 Å for Zr ions [40], it is suggested that the $\langle Zr-O \rangle$ bonds exhibit weaker ionicity than $\langle Pu-O \rangle$ bonds in $Gd_2Zr_{2-y}Pu_yO_7$. Because of the brittleness of the ionic bonds, the immobilization of Pu at Zr sites will thus increase the ionicity and decrease the elastic moduli.

Table 4. Bader charge (|e|) for each ion in $Gd_{2-y}Pu_yZr_2O_7$ and $Gd_2Zr_{2-y}Pu_yO_7$ ($y = 0, 0.5, 1.0, 1.5, 2.0$).

	Gd	Pu	Zr	O _{48f}	O _{8b}
$Gd_2Zr_2O_7$	2.16	-	2.26	-1.25	-1.37
$Gd_{1.5}Pu_{0.5}Zr_2O_7$	2.15	2.10	2.27	-1.25	-1.35
$Gd_{1.0}Pu_{1.0}Zr_2O_7$	2.13	2.11	2.27	-1.24	-1.35
$Gd_{0.5}Pu_{1.5}Zr_2O_7$	2.15	2.09	2.28	-1.24	-1.33
$Pu_2Zr_2O_7$	-	2.08	2.27	-1.23	-1.32
$Gd_2Zr_{1.5}Pu_{0.5}O_7$	2.14	2.36	2.26	-1.25	-1.37
$Gd_2Zr_{1.0}Pu_{1.0}O_7$	2.15	2.31	2.27	-1.25	-1.37
$Gd_2Zr_{0.5}Pu_{1.5}O_7$	2.15	2.34	2.24	-1.25	-1.36
$Gd_2Pu_2O_7$	2.16	2.30	-	-1.26	-1.38

3.3. Ductility, Elastic Anisotropy, Debye Temperature and Electronic Structures of Pu-Doped $Gd_2Zr_2O_7$

Pugh's indicator ($\frac{B}{G}$) is used to reflect the ductility of materials. If $\frac{B}{G} > 1.75$, the material shows ductility; or, it is brittle [54]. Table 5 presents the calculated Pugh's indicators. For $Gd_2Zr_2O_7$, our value of 1.907 is comparable with the experimental values of 1.913 [45,46], 1.891 [20] and other calculated value of 2.004 [53]. For both $Gd_{2-y}Pu_yZr_2O_7$ and $Gd_2Zr_{2-y}Pu_yO_7$, our calculations show that the Pugh's indicators are all larger than 1.75, implying that all the considered composites are ductile. Poisson's indicator (ν) can be employed to evaluate the relative ductility of materials. When ν is around 0.1, the material shows brittle covalent properties. When ν is bigger than 0.25, it exhibits ductile ionic properties [55]. Table 5 lists the calculated, experimental and others' calculated Poisson's ratio for both $Gd_{2-y}Pu_yZr_2O_7$ and $Gd_2Zr_{2-y}Pu_yO_7$. For $Gd_2Zr_2O_7$, the calculated Poisson's ratio of 0.277 could be comparable to the experimental values of 0.276 [45,46], 0.274 [20] and other calculated results of 0.286 [53] and 0.273 [43]. The Poisson's ratios for $Gd_{2-y}Pu_yZr_2O_7$ and $Gd_2Zr_{2-y}Pu_yO_7$ are all larger than 0.25, as presented in Table 5, i.e., the Pu-substituted $Gd_2Zr_2O_7$ exhibit good ductility.

Table 5. Pugh's indicator (B/G), elastic anisotropy index (A^U), sound wave velocity (v_m , in m/s), Debye temperature (θ , in K) and Poisson's ratio (ν) of $Gd_{2-y}Pu_yZr_2O_7$ and $Gd_2Zr_{2-y}Pu_yO_7$ ($0 \leq y \leq 2$).

		B/G	A^U	v_m	θ	ν
$Gd_2Zr_2O_7$		1.907	0.01355	4666.0	580.2	0.277
	Exp. [45,46]	1.913				0.276
	Exp. [20]	1.891			513.3	0.274
	Cal. [53]	2.004	0.00420	4833.5	612.9	0.286
	Cal. [43]					0.273
$Gd_{1.5}Pu_{0.5}Zr_2O_7$		1.931	0.00598	4533.7	560.7	0.279
$Gd_{1.0}Pu_{1.0}Zr_2O_7$		1.950	0.00105	4367.8	540.2	0.281
$Gd_{0.5}Pu_{1.5}Zr_2O_7$		1.964	0.00032	4247.4	522.5	0.282
$Pu_2Zr_2O_7$		1.987	0.00004	4106.4	503.8	0.285
$Gd_2Zr_{1.5}Pu_{0.5}O_7$		1.928	0.04881	4124.6	508.7	0.279
$Gd_2Zr_{1.0}Pu_{1.0}O_7$		2.278	0.21353	3591.7	439.5	0.309
$Gd_2Zr_{0.5}Pu_{1.5}O_7$		2.243	0.10062	3590.2	435.9	0.306
$Gd_2Pu_2O_7$		2.151	0.06923	3471.3	418.3	0.299

Elastic anisotropy is an important parameter for phase transformations, dislocation dynamics and geophysical applications [56]. Ranganathan and co-workers [57,58] proposed the universal elastic anisotropic index to indicate the elastic anisotropy of cubic crystals. The index $A^U = 5\frac{G^V}{C^V} + \frac{B^V}{B^R} - 6$ is investigated for all the considered compositions, where $A^U = 0$ describes an isotropic crystal [57,58]. The calculated A^U for both $Gd_{2-y}Pu_yZr_2O_7$ and $Gd_2Zr_{2-y}Pu_yO_7$ are shown in Table 5. For $Gd_2Zr_2O_7$, our calculated value of 0.01355 is comparable with other calculated value of 0.00420 [53]. As Pu is immobilized at Gd-site, we find that the A^U values for all the compositions are nearly zero, indicating that the $Gd_{2-y}Pu_yZr_2O_7$ compounds are isotropic elastically. As for the immobilization of Pu at Zr-site, the A^U values are 0.21353 for $Gd_2Zr_{1.0}Pu_{1.0}O_7$ and 0.10062 for $Gd_2Zr_{0.5}Pu_{1.5}O_7$, indicative of elastic anisotropy.

The thermal properties of materials can be analyzed by the Debye temperature [4]. Table 5 lists the calculated and available experimental Debye temperature. The calculated θ_D value of 580.2 K for $Gd_2Zr_2O_7$ is larger than the experimental result of 513.3 K [20], but shows better agreement with experimental value than another calculated value of 612.9 K [53]. As the Pu concentration increases, the θ_D value decreases for both $Gd_{2-y}Pu_yZr_2O_7$ and $Gd_2Zr_{2-y}Pu_yO_7$. In particular, the θ_D values for $Gd_2Zr_{2-y}Pu_yO_7$ are smaller than those for $Gd_{2-y}Pu_yZr_2O_7$. These results imply that the $Gd_2Zr_{2-y}Pu_yO_7$ compositions have a lower melting point and weaker interatomic binding force than the $Gd_{2-y}Pu_yZr_2O_7$ compositions. Zhao et al. [59] calculated the Debye temperature for Th immobilization at Gd-site and Zr-site of $Gd_2Zr_2O_7$ and observed similar phenomena, i.e., the Th-substituted $Gd_2Zr_2O_7$ have a lower Debye temperature and especially smaller Debye temperature can be obtained by the Th immobilization at Zr-site than that at Gd-site.

The total and projected density of state (DOS) distributions for $Gd_{2-y}Pu_yZr_2O_7$ and $Gd_2Zr_{2-y}Pu_yO_7$ are illustrated in Figures 6 and 7, respectively. Tables 1 and 2 list the band gap values. It is shown that all the compositions have large band gap values. For $Gd_2Zr_2O_7$, the calculated band gap is 2.86 eV. For Pu incorporation into Gd-site, the band gap values of 2.27–2.37 eV are smaller than that of $Gd_2Zr_2O_7$ and nearly independent of the Pu content. For $Gd_2Zr_{2-y}Pu_yO_7$, the changes in the band gap is more significant, ranging from 2.33 to 1.68 eV. It is indicated that Pu immobilization at Gd-site and Zr-site has different influences on the electronic structure of $Gd_2Zr_2O_7$. The same conclusion can be drawn from the density of state distribution. For $Gd_{2-y}Pu_yZr_2O_7$, O 2p orbital dominates and hybridizes with very few Gd 5d, Pu 5f and Zr 4d orbitals in the energy range of -5 – -1 eV, and the Pu 5f orbitals hybridize with the O 2p orbitals at the bottom of valence band. For $Gd_2Zr_{2-y}Pu_yO_7$, the O 2p orbital dominates and hybridizes with Pu 5f orbitals and very few Zr 4d and Gd 5d orbitals at the valence band. Obviously, in $Gd_2Zr_2O_7$, different electronic structures can be obtained from the immobilization of Pu at Gd and Zr sites. These different electronic structures may result in discrepancies in the thermo-physical properties of $Gd_{2-y}Pu_yZr_2O_7$ and $Gd_2Zr_{2-y}Pu_yO_7$.

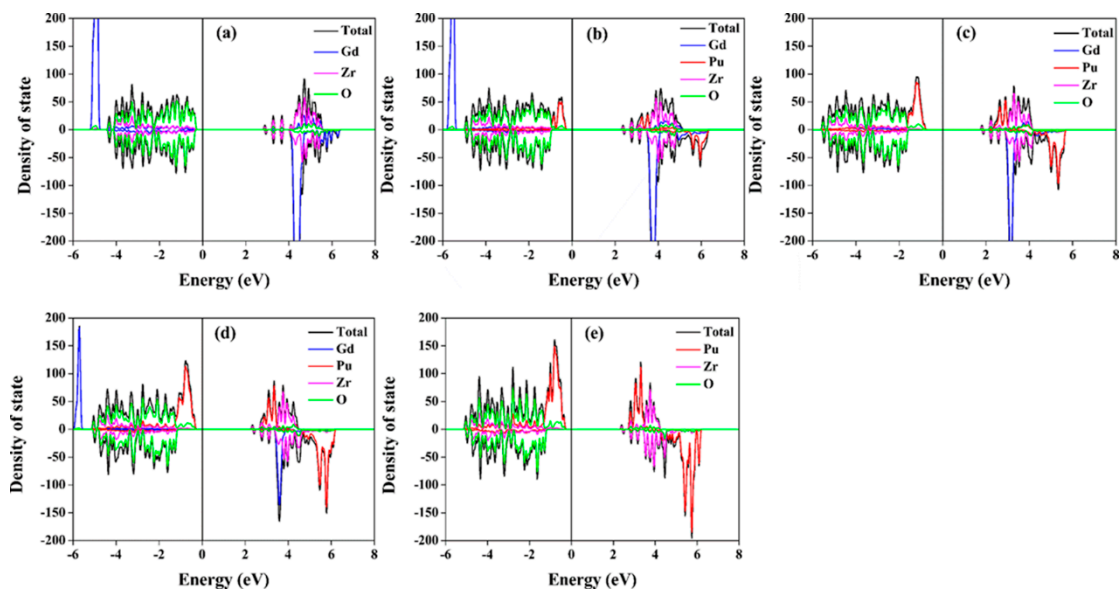


Figure 6. Total and projected density of state distributions for: (a) $Gd_2Zr_2O_7$; (b) $Gd_{1.5}Pu_{0.5}Zr_2O_7$; (c) $Gd_{1.0}Pu_{1.0}Zr_2O_7$; (d) $Gd_{0.5}Pu_{1.5}Zr_2O_7$; (e) $Pu_2Zr_2O_7$.

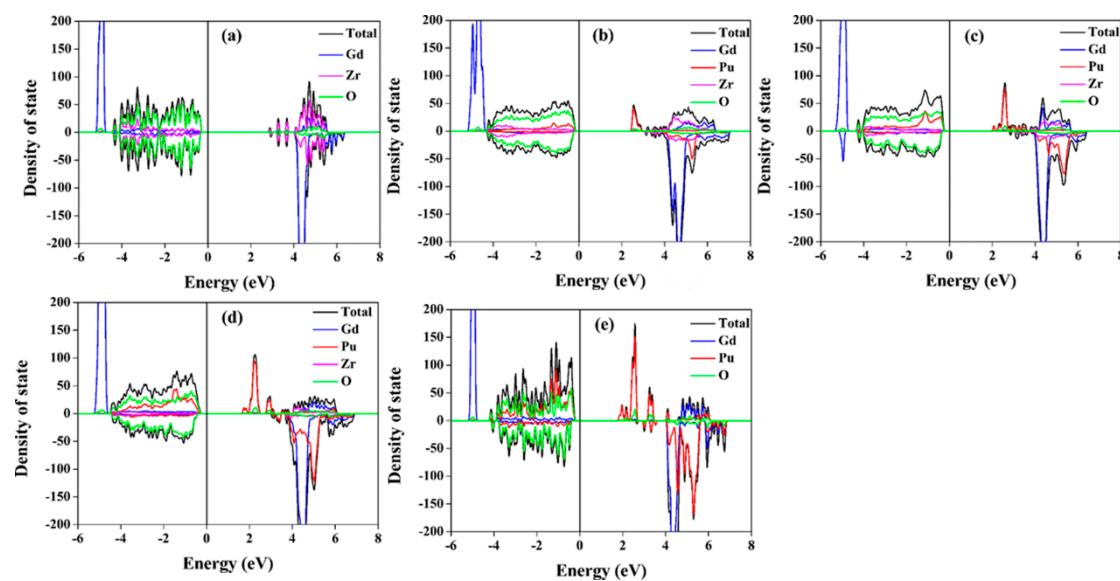


Figure 7. Total and projected density of state distributions for: (a) $Gd_2Zr_2O_7$; (b) $Gd_2Zr_{1.5}Pu_{0.5}O_7$; (c) $Gd_2Zr_{1.0}Pu_{1.0}O_7$; (d) $Gd_2Zr_{0.5}Pu_{1.5}O_7$; (e) $Gd_2Pu_2O_7$.

4. Conclusions

The mechanical and electronic properties of Pu-containing $Gd_2Zr_2O_7$ are studied by a DFT+U method. For $Gd_{2-y}Pu_yZr_2O_7$ and $Gd_2Zr_{2-y}Pu_yO_7$, the elastic stability criteria are satisfied for all the calculated elastic constants, i.e., all the compounds are mechanically stable. As Pu immobilizes at Gd-site in $Gd_2Zr_2O_7$, because the bonding distance and covalency of $\langle Gd-O \rangle$ and $\langle Pu-O \rangle$ bonds are comparable to each other, the elastic constants, elastic moduli, elastic isotropy and Debye temperature of $Gd_2Zr_2O_7$ are all affected a little. As for $Gd_2Zr_{2-y}Pu_yO_7$, the elastic constants and elastic moduli change remarkably as compared with $Gd_2Zr_2O_7$. The substitution of Pu for Zr sites increases the ionicity and decreases the elastic moduli, because the $\langle Zr-O \rangle$ bonds exhibit weaker ionicity than $\langle Pu-O \rangle$ bonds. In addition, the Debye temperature is decreased and the band gap is greatly reduced. Our calculations suggest that the $Gd_2Zr_2O_7$ is a promising material for immobilizing nuclear waste

such as Pu, while the thermo-physical of $Gd_2Zr_2O_7$ may be influenced significantly after nuclear waste incorporation.

Author Contributions: Conceptualization, H.X.; Methodology, H.X. and P.L.; Validation, H.X. and F.Z.; Investigation, P.L.; Data Curation, P.L., F.Z. and S.Z.; Writing—Original Draft Preparation, P.L.; Writing—Review & Editing, H.Z., H.G., Z.L. and X.Z.; Supervision, H.X.

Acknowledgments: H.X. was supported by NSAF Joint Foundation of China (Grant No. U1530129). Z.L. was supported by National Natural Science Foundation of China (Grant No. 11464025), the New Century Excellent Talents in University under Grant No. NECT-11-0906 and the Key Talent Foundation of Gansu Province. The theoretical calculations were performed using the supercomputer resources at TianHe-1 located at National Supercomputer Center in Tianjin.

Conflicts of Interest: The authors declare no conflict of interest.

References

1. Ewing, R.C. Nuclear waste forms for actinides. *Proc. Natl. Acad. Sci. USA* **1999**, *96*, 3432–3439. [[CrossRef](#)] [[PubMed](#)]
2. Xiao, H.Y.; Jiang, M.; Zhao, F.A.; Liu, Z.J.; Zu, X.T. Thermal and mechanical stability, electronic structure and energetic properties of Pu-containing pyrochlores: $La_{2-y}Pu_yZr_2O_7$ and $La_2Zr_{2-y}Pu_yO_7$ ($0 \leq y \leq 2$). *J. Nucl. Mater.* **2015**, *466*, 162–171. [[CrossRef](#)]
3. Ewing, R.C.; Weber, W.J.; Lian, J. Nuclear waste disposal—Pyrochlore ($A_2B_2O_7$): Nuclear waste form for the immobilization of plutonium and “minor” actinides. *J. Appl. Phys.* **2004**, *95*, 5949–5971. [[CrossRef](#)]
4. Kittel, C. *Introduction to Solid State Physics*, 6th ed.; John Wiley & Sons, Inc.: New York, NY, USA, 1986; pp. 106–107.
5. Chroneos, A.; Rushton, M.J.D.; Jiang, C.; Tsoukalas, L.H. Nuclear wasteform materials: Atomistic simulation case studies. *J. Nucl. Mater.* **2013**, *441*, 29–39. [[CrossRef](#)]
6. Wang, S.X.; Begg, B.D.; Wang, L.M.; Ewing, R.C.; Weber, W.J.; Kutty, K.V.G. Radiation stability of gadolinium zirconate: A waste form for plutonium disposition. *J. Mater. Res.* **1999**, *14*, 4470–4473. [[CrossRef](#)]
7. Sickafus, K.E.; Minervini, L.; Grimes, R.W.; Valdez, J.A.; Ishimaru, M.; Li, F.; McClellan, K.J.; Hartmann, T. Radiation tolerance of complex oxides. *Science* **2000**, *289*, 748–751. [[CrossRef](#)] [[PubMed](#)]
8. Weber, W.J. Plutonium immobilization and radiation effects. *Science* **2000**, *289*, 2051–2052. [[CrossRef](#)]
9. Devanathan, R.; Weber, W.J.; Gale, J.D. Radiation tolerance of ceramics—Insights from atomistic simulation of damage accumulation in pyrochlores. *Energy Environ. Sci.* **2010**, *3*, 1551–1559. [[CrossRef](#)]
10. Patwe, S.J.; Tyagi, A.K. Solubility of Ce^{4+} and Sr^{2+} in the pyrochlore lattice of $Gd_2Zr_2O_7$ for simulation of Pu and alkaline earth metal. *Ceram. Int.* **2006**, *32*, 545–548. [[CrossRef](#)]
11. Mandal, B.P.; Tyagi, A.K. Pyrochlores: Potential multifunctional materials. *BARC Newslett.* **2010**, *313*, 6–13.
12. Zhao, P.Z.; Li, L.Y.; Xu, S.M.; Zhang, Q. Synthesis and structural transformations of $(Gd_{1-x}Ce_x)_2Zr_2O_{7+x}$: An analogue for Pu immobilization. *Acta Phys. Chim. Sin.* **2013**, *29*, 1168–1172.
13. Reid, D.P.; Stennett, M.C.; Hyatt, N.C. The fluorite related modulated structures of the $Gd_2(Zr_{2-x}Ce_x)O_7$ solid solution: An analogue for Pu disposition. *J. Solid State Chem.* **2012**, *191*, 2–9. [[CrossRef](#)]
14. Patwe, S.J.; Ambekar, B.R.; Tyagi, A.K. Synthesis, characterization and lattice thermal expansion of some compounds in the system $Gd_2Ce_xZr_{2-x}O_7$. *J. Alloys Compd.* **2005**, *389*, 243–246. [[CrossRef](#)]
15. Zhao, F.A.; Xiao, H.Y.; Jiang, M.; Liu, Z.J.; Zu, X.T. A DFT+U study of Pu immobilization in $Gd_2Zr_2O_7$. *J. Nucl. Mater.* **2015**, *467*, 937–948. [[CrossRef](#)]
16. Williford, R.E. Computer simulation of Pu^{3+} and Pu^{4+} substitutions in gadolinium zirconate. *J. Nucl. Mater.* **2001**, *299*, 140–147. [[CrossRef](#)]
17. Cleave, A.; Grimes, R.W.; Sickafus, K. Plutonium and uranium accommodation in pyrochlore oxides. *Philos. Mag.* **2005**, *85*, 967–980. [[CrossRef](#)]
18. Wang, X.J.; Xiao, H.Y.; Zu, X.T.; Weber, W.J. Study of cerium solubility in $Gd_2Zr_2O_7$ by DFT + U calculations. *J. Nucl. Mater.* **2011**, *419*, 105–111. [[CrossRef](#)]
19. Wang, Y.; Yang, F.; Xiao, P. Role and determining factor of substitutional defects on thermal conductivity: A study of $La_2(Zr_{1-x}B_x)_2O_7$ ($B = Hf, Ce, 0 \leq x \leq 0.5$) pyrochlore solid solutions. *Acta Mater.* **2014**, *68*, 106–115. [[CrossRef](#)]

20. Shimamura, K.; Arima, T.; Idemitsu, K.; Inagaki, Y. Thermophysical properties of rare-earth-stabilized zirconia and zirconate pyrochlores as surrogates for actinide-doped zirconia. *Int. J. Thermophys.* **2007**, *28*, 1074–1084. [[CrossRef](#)]
21. Kresse, G.; Furthmüller, J. Efficiency of ab-initio total energy calculations for metals and semiconductors using a plane-wave basis set. *Comput. Mater. Sci.* **1996**, *6*, 15–50. [[CrossRef](#)]
22. Kresse, G.; Furthmüller, J. Efficient iterative schemes for ab initio total-energy calculations using a plane-wave basis set. *Phys. Rev. B* **1996**, *54*, 11169–11186. [[CrossRef](#)]
23. Dudarev, S.L.; Botton, G.A.; Savrasov, S.Y.; Humphreys, C.J.; Sutton, A.P. Electron-energy-loss spectra and the structural stability of nickel oxide: An LSDA+U study. *Phys. Rev. B* **1998**, *57*, 1505–1509. [[CrossRef](#)]
24. Blöchl, P.E. Projector augmented-wave method. *Phys. Rev. B* **1994**, *50*, 17953–17979. [[CrossRef](#)]
25. Wu, Z.; Cohen, R.E. More accurate generalized gradient approximation for solids. *Phys. Rev. B* **2006**, *73*, 235116. [[CrossRef](#)]
26. Constantin, L.A.; Terentjevs, A.; Della Sala, F.; Fabiano, E. Gradient-dependent upper bound for the exchange-correlation energy and application to density functional theory. *Phys. Rev. B* **2015**, *91*, 041120(R). [[CrossRef](#)]
27. Constantin, L.A.; Terentjevs, A.; Della Sala, F.; Cortona, P.; Fabiano, E. Semiclassical atom theory applied to solid-state physics. *Phys. Rev. B* **2016**, *93*, 045126. [[CrossRef](#)]
28. Perdew, J.P.; Burke, K.; Ernzerhof, M. Generalized gradient approximation made simple. *Phys. Rev. Lett.* **1996**, *77*, 3865–3868. [[CrossRef](#)]
29. Wei, S.H.; Ferreira, L.G.; Bernard, J.E.; Zunger, A. Electronic properties of random alloys: Special quasirandom structures. *Phys. Rev. B* **1990**, *42*, 9622–9649. [[CrossRef](#)]
30. Zunger, A.; Wei, S.; Ferreira, L.G.; Bernard, J.E. Special quasirandom structures. *Phys. Rev. Lett.* **1990**, *65*, 353–356. [[CrossRef](#)]
31. Jiang, C.; Wolverton, C.; Sofu, J.; Chen, L.Q.; Liu, Z.K. First-principles study of binary bcc alloys using special quasirandom structures. *Phys. Rev. B* **2004**, *69*, 214202. [[CrossRef](#)]
32. Jiang, C.; Stanek, C.R.; Sickafus, K.E.; Uberuaga, B.P. First-principles prediction of disordering tendencies in pyrochlore oxides. *Phys. Rev. B* **2009**, *79*, 104203. [[CrossRef](#)]
33. McCleskey, T.M.; Bauer, E.; Jia, Q.; Burrell, A.K.; Scott, B.L.; Conradson, S.D.; Mueller, A.; Roy, L.; Wen, X.; Scuseria, G.E.; et al. Optical band gap of NpO₂ and PuO₂ from optical absorbance of epitaxial films. *J. Appl. Phys.* **2013**, *113*. [[CrossRef](#)]
34. Chikalla, T.D.; McNeilly, C.E.; Skavdahl, R.E. The plutonium-oxygen system. *J. Nucl. Mater.* **1964**, *12*, 131–141. [[CrossRef](#)]
35. Jomard, G.; Amadon, B.; Bottin, F.; Torrent, M. Structural, thermodynamic, and electronic properties of plutonium oxides from first principles. *Phys. Rev. B* **2008**, *78*, 075125. [[CrossRef](#)]
36. Sun, B.; Zhang, P.; Zhao, X.-G. First-principles local density approximation plus U and generalized gradient approximation plus U study of plutonium oxides. *J. Chem. Phys.* **2008**, *128*, 084705. [[CrossRef](#)] [[PubMed](#)]
37. Wen, X.-D.; Martin, R.L.; Henderson, T.M.; Scuseria, G.E. Density Functional Theory Studies of the Electronic Structure of Solid State Actinide Oxides. *Chem. Rev.* **2013**, *113*, 1063–1096. [[CrossRef](#)] [[PubMed](#)]
38. Mandal, B.P.; Banerji, A.; Sathe, V.; Deb, S.K.; Tyagi, A.K. Order–disorder transition in Nd_{2–y}Gd_yZr₂O₇ pyrochlore solid solution: An X-ray diffraction and Raman spectroscopic study. *J. Solid State Chem.* **2007**, *180*, 2643–2648. [[CrossRef](#)]
39. Yamazaki, S.; Yamashita, T.; Matsui, T.; Nagasaki, T. Thermal expansion and solubility limits of plutonium-doped lanthanum zirconates. *J. Nucl. Mater.* **2001**, *294*, 183–187. [[CrossRef](#)]
40. Shannon, R.D. Revised effective ionic radii and systematic studies of interatomic distances in halides and chalcogenides. *Acta Crystallogr. Sect. A Cryst. Phys. Diffr. Theor. Gen. Crystallogr.* **1976**, *32*, 751–767. [[CrossRef](#)]
41. Lian, J.; Zu, X.T.; Kutty, K.V.G.; Chen, J.; Wang, L.M.; Ewing, R.C. Ion-irradiation-induced amorphization of La₂Zr₂O₇ pyrochlore. *Phys. Rev. B* **2002**, *66*, 054108. [[CrossRef](#)]
42. Ravindran, P.; Fast, L.; Korzhavyi, P.A.; Johansson, B.; Wills, J.; Eriksson, O. Density functional theory for calculation of elastic properties of orthorhombic crystals: Application to TiSi₂. *J. Appl. Phys.* **1998**, *84*, 4891–4904. [[CrossRef](#)]
43. Lan, G.; Ouyang, B.; Song, J. The role of low-lying optical phonons in lattice thermal conductance of rare-earth pyrochlores: A first-principle study. *Acta Mater.* **2015**, *91*, 304–317. [[CrossRef](#)]

44. Zhang, P.; Wang, B.T.; Zhao, X. Ground-state properties and high-pressure behavior of plutonium dioxide: Density functional theory calculations. *Phys. Rev. B* **2010**, *82*, 144110. [[CrossRef](#)]
45. Van Dijk, M.P.; de Vries, K.J.; Burggraaf, A.J. Oxygen ion and mixed conductivity in compounds with the fluorite and pyrochlore structure. *Solid State Ion.* **1983**, *9*, 913–919. [[CrossRef](#)]
46. Wu, J.; Wei, X.; Padtur, N.P.; Klemens, P.G.; Gell, M.; Garcia, E.; Miranzo, P.; Osendi, M.I. Low-thermal-conductivity rare-earth zirconates for potential thermal-barrier-coating applications. *J. Am. Ceram. Soc.* **2002**, *85*, 3031–3035. [[CrossRef](#)]
47. Zhao, F.A.; Xiao, H.Y.; Bai, X.M.; Liu, Z.J.; Zu, X.T. Effects of Nd doping on the mechanical properties and electronic structures of $Gd_2Zr_2O_7$: A first-principles-based study. *J. Mater. Sci.* **2018**, *53*, 16423–16438. [[CrossRef](#)]
48. Chung, D.H. Elastic moduli of single crystal and polycrystalline MgO. *Philos. Mag.* **1963**, *8*, 833–841. [[CrossRef](#)]
49. Voigt, W. Ueber die Beziehung zwischen den beiden Elasticitätsconstanten isotroper Körper. *Annalen der Physik* **1889**, *274*, 573–587. [[CrossRef](#)]
50. Reuss, A. Account of the liquid limit of mixed crystals on the basis of the plasticity condition for single crystal. *Z. Angew. Math. Mech.* **1929**, *9*, 49–58. [[CrossRef](#)]
51. Hill, R. The elastic behaviour of a crystalline aggregate. *Proc. Phys. Soc. Sect. A* **1952**, *65*, 349. [[CrossRef](#)]
52. Liu, B.; Wang, J.Y.; Li, F.Z.; Zhou, Y.C. Theoretical elastic stiffness, structural stability and thermal conductivity of $La_2T_2O_7$ (T = Ge, Ti, Sn, Zr, Hf) pyrochlore. *Acta Mater.* **2010**, *58*, 4369–4377. [[CrossRef](#)]
53. Zhang, S.; Zhang, H.B.; Zhao, F.A.; Jiang, M.; Xiao, H.Y.; Liu, Z.J.; Zu, X.T. Impact of isovalent and aliovalent substitution on the mechanical and thermal properties of $Gd_2Zr_2O_7$. *Sci. Rep.* **2017**, *7*, 6399. [[CrossRef](#)] [[PubMed](#)]
54. Pugh, S.F. XCII. Relations between the elastic moduli and the plastic properties of polycrystalline pure metals. *Lond. Edinb. Dublin Philos. Mag. J. Sci.* **2009**, *45*, 823–843. [[CrossRef](#)]
55. Fine, M.E.; Brown, L.D.; Marcus, H.L. Elastic constants versus melting temperature in metals. *Scr. Metall.* **1984**, *18*, 951–956. [[CrossRef](#)]
56. Ledbetter, H.; Migliori, A. A general elastic-anisotropy measure. *J. Appl. Phys.* **2006**, *100*, 063516. [[CrossRef](#)]
57. Ranganathan, S.I.; Ostoja-Starzewski, M. Universal elastic anisotropy index. *Phys. Rev. Lett.* **2008**, *101*, 055504. [[CrossRef](#)] [[PubMed](#)]
58. Feng, J.; Xiao, B.; Wan, C.L.; Qu, Z.X.; Huang, Z.C.; Chen, J.C.; Zhou, R.; Pan, W. Electronic structure, mechanical properties and thermal conductivity of $Ln_2Zr_2O_7$ (Ln = La, Pr, Nd, Sm, Eu and Gd) pyrochlore. *Acta Mater.* **2011**, *59*, 1742–1760. [[CrossRef](#)]
59. Zhao, F.A.; Xiao, H.Y.; Liu, Z.J.; Li, S.; Zu, X.T. A DFT study of mechanical properties, thermal conductivity and electronic structures of Th-doped $Gd_2Zr_2O_7$. *Acta Mater.* **2016**, *121*, 299–309. [[CrossRef](#)]

